2000 J. Med. Chem. 2010, 53, 2000–2009
DOI: 10.1021/jm901453q

Journal of Medicinal Chemistry Article

Discovery of 7-(4-(3-Ethynylphenylamino)-7-methoxyquinazolin-6-yloxy)-*N*-hydroxyheptanamide (CUDC-101) as a Potent Multi-Acting HDAC, EGFR, and HER2 Inhibitor for the Treatment of Cancer

Xiong Cai,* Hai-Xiao Zhai, Jing Wang, Jeffrey Forrester, Hui Qu, Ling Yin, Cheng-Jung Lai, Rudi Bao, and Changgeng Qian

Curis Inc., 45 Moulton Street, Cambridge, Massachusetts 02138

Received October 1, 2009

By incorporating histone deacetylase (HDAC) inhibitory functionality into the pharmacophore of the epidermal growth factor receptor (EGFR) and human epidermal growth factor receptor 2 (HER2) inhibitors, we synthesized a novel series of compounds with potent, multiacting HDAC, EGFR, and HER2 inhibition and identified 7-(4-(3-ethynylphenylamino)-7-methoxyquinazolin-6-yloxy)-*N*-hydroxyheptanamide **8** (CUDC-101) as a drug candidate, which is now in clinical development. **8** displays potent in vitro inhibitory activity against HDAC, EGFR, and HER2 with an IC_{50} of 4.4, 2.4, and 15.7 nM, respectively. In most tumor cell lines tested, **8** exhibits efficient antiproliferative activity with greater potency than vorinostat (SAHA), erlotinib, lapatinib, and combinations of vorinostat/erlotinib and vorinostat/lapatinib. In vivo, **8** promotes tumor regression or inhibition in various cancer xenograft models including nonsmall cell lung cancer (NSCLC), liver, breast, head and neck, colon, and pancreatic cancers. These results suggest that a single compound that simultaneously inhibits HDAC, EGFR, and HER2 may offer greater therapeutic benefits in cancer over single-acting agents through the interference with multiple pathways and potential synergy among HDAC and EGFR/HER2 inhibitors.

Introduction

The human epidermal growth factor receptor (HER) family of receptor tyrosine kinases (RTKs[a]) is recognized as a key mediator of cancer progression.[1−4] The HER tyrosine kinase family consists of four structurally related cellular receptors: the epidermal growth factor receptor (EGFR; HER1), HER2 (ErbB2), HER3 (ErbB3), and HER4.[2,5] The EGFR inhibitors erlotinib and gefitinib as well as the dual EGFR/HER2 inhibitor lapatinib (Chart 1) are FDA-approved cancer drugs that are effective against multiple solid tumor cancers.[6] However, their efficacy is restricted to a small subset of patients due to molecular heterogeneity among and within tumors.[7,8] Their effectiveness is also limited by the drug resistance that frequently emerges following treatment.[9,10]

To overcome the low response rate and acquired resistance to RTK inhibitors, a number of strategies have been tested, including combination therapies and multitargeted inhibitors to inhibit multiple pathogenic pathways.[11] One particularly promising approach is the modulation of RTK pathways by the inhibition of histone deacetylases (HDACs). HDACs comprise a family of 18 genes in humans and are divided into four classes.[12] Among them are the Class I (HDAC1, HDAC2, HDAC3, and HDAC8) and II (HDAC4, HDAC5, HDAC6, HDAC7, HDAC9, and HDAC10) zinc-containing hydrolases. HDAC inhibitors can impact a variety of cell functions by blocking the deacetylation of histone or nonhistone proteins, such as HSP90 and tubulin, causing cell cycle arrest, differentiation, and/or apoptosis.[13] The HDAC inhibitor vorinostat (SAHA) (Chart 1) is an FDA-approved drug for the treatment of cutaneous T-cell lymphoma (CTCL).[14]

HDAC inhibitors have also been shown to synergize with other agents, including RTK inhibitors, to suppress proliferation and induce apoptosis in tumor cells.[15−21] In our own study, two reference compounds, vorinostat and erlotinib, were used to achieve HDAC and EGFR inhibition, respectively, and a well-established mathematical model for studying multidrug interactions[22] was applied to assess whether there is a synergistic effect between HDAC and RTK inhibition.[20] Using this mathematical model, IC50s of growth inhibition of several cancer cells treated with vorinostat, erlotinib, or their combination were compared, and combination indices were calculated to interpret the effect of concurrent inhibition of the HDAC and RTK targets. Our results show that cotreatment with vorinostat and erlotinib (1:1 ratio) results in greater growth inhibition and with combination indices well below 1, indicating considerable synergy between the inhibition of these two targets (Supporting Information Table S1). We also carried out similar studies by applying varying ratios of vorinostat and erlotinib. In all cases, the combination indices were calculated to be well below 1,[20] indicating that the inhibition between these two targets is synergistic and that this synergy is not affected by the specific dosing ratio. This result suggests that a single molecule that simultaneously inhibits HDAC and RTK activities could act synergistically in treated cancer cells. With

*To whom correspondence should be addressed. Phone: 617-503-6656. Fax: 617-503-6501. E-mail: xcai@curis.com.

[a] Abbreviations: HDAC(s), histone deacetylase(s); RTKs, receptor tyrosine kinases; EGFR, epidermal growth factor receptor; HER, human epidermal growth factor receptor; HER2, human epidermal growth factor receptor 2; NSCLC, nonsmall cell lung cancer; HNSCC, head and neck squamous cell carcinoma; CTCL, cutaneous T-cell lymphoma; SAR, structure−activity relationship; HDLP, HDAC like protein; PK, pharmacokinetics; PD, pharmacodynamics; MTD, maximum tolerated dose; PDB, protein data bank.

 Published on Web 02/09/2010

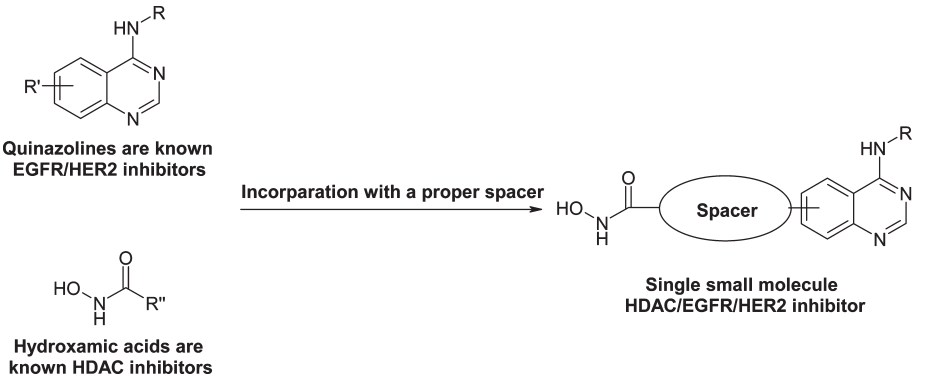

Figure 1. Design of multitargeted EGFR/HER2/HDAC inhibitors.

Chart 1. Structure of Known Inhibitors

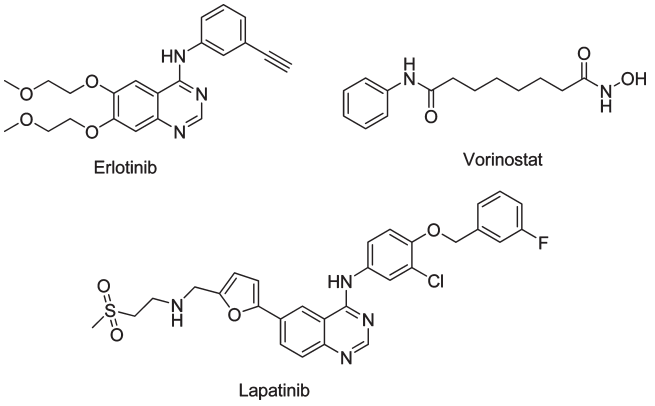

combined inhibitory activities and synergistic effects, such a multiacting single molecule may not only enhance drug efficacy but also overcome the current clinical limitations of EGFR/HER2 inhibitors, such as poor overall response rates and the rapid emergence of drug resistance. Unlike combinations of two or more EGFR/HER2 and HDAC inhibitors, a single agent with EGFR/HER2 and HDAC inhibitory activities offers key advantages, including concurrent pharmacokinetics, minimized off-target adverse effects, and drug−drug interactions caused by multiple agents, as well as increased patient compliance and reduced drug cost.

Investigating the structural requirements of EGFR/HER2 and HDAC inhibitors led us to design and synthesize a series of novel, potent multitargeted inhibitors. Here, we describe the design, synthesis, and structure−activity relationship (SAR) of these novel compounds and the identification of **8** (CUDC-101) as a clinical candidate currently in phase I clinical trials.

Compound Design

Several EGFR, HER2, and HDAC inhibitors have been reported.[23,24] These studies reveal hydroxamic acid as a broad class of HDAC inhibitors with high affinity for HDACs that depend on zinc chelation for their activity.[25] Additionally, quinazolines are a well-characterized scaffold of kinase inhibitors, including EGFR and HER2 inhibitors.[26] The X-ray cocrystal structures of EGFR with erlotinib and HDAC with vorinostat have been reported.[24,27,28] Our compound design strategy was to fully analyze the structure requirements of these ligand−protein interactions and design our own novel multitargeted inhibitors through a structure-based rational drug design approach. It has been reported that erlotinib binds to the EGFR binding domain with quinazoline occupying the adenine region of the ATP binding site and forming two hydrogen bonds at N1 and N3, the phenyl-amino group occupying the hydrophobic pocket, and the two methoxy-ethoxy groups at C-6 and C-7 of the quinazoline ring sticking out of the receptor.[24,27] The cocrystal structure of trichostatin A (TSA) or vorinostat with HDLP (an HDAC-like protein) reveals that both compounds bind to HDLP with their large hydrophobic groups (phenyl) binding to the hydrophobic part of the enzyme, the aliphatic chain sitting in the 11 Å tube-like channel through multiple contacts with hydrophobic residues, and the terminal hydroxamic acid interacting with zinc at the active site to disrupt enzyme activity.[28,29] Since the methoxy-ethoxy groups extend outside of the EGFR binding pocket and are flexible, we reasoned that the modification of these side chains should not dramatically affect binding to EGFR. Through careful analysis of the ligand−protein interactions, we deduced that a group containing a side-chain of a certain length that terminates with a hydroxamic acid is essential for HDAC binding and that such a group is well-suited to be incorporated into the quinazoline-based EGFR/HER2 inhibitors. We predicted that the best place to introduce hydroxamic acid functionality without sacrificing EGFR/HER2 binding affinity is the site in which the methoxy-ethoxy groups of erlotinib are located (C-6 or C-7 of the quinazoline ring). We also predicted that the hydrophobic pocket within the HDAC dimeric interface should be large enough to accommodate the phenylaminoquinazoline backbone of EGFR/HER2 inhibitors, and that the incorporated side chain with the terminal hydroxamic acid should be able to reach the active site and interact with zinc as required to disrupt the HDAC enzyme activity. Therefore, to obtain and optimize HDAC, EGFR, and HER2 inhibitory activities in a single molecule, we incorporated hydroxamic acid functionality into the quinazoline pharmacophore of EGFR/HER2 inhibitors with a proper spacer, which served as a bridge to properly display HDAC and EGFR/HER2 inhibitory pharmacophores (Figure 1). This novel design strategy proved to be highly effective in producing single molecules with potent multiacting HDAC/EGFR/HER2 inhibition and low molecular weights.

Chemistry

The preparation of analogues with various chain lengths and aniline substitution (**1**−**11**) is shown in Scheme 1. Compounds **31**−**35** were prepared through the coupling of anilines **27**−**30** with either quinazolines **25**[30] or **26**.[31] Hydrolysis of the acetyl group on C-6 of compounds **31**−**35** using lithium hydroxide gave corresponding C6-OH quinazolines **36**−**40**. Alkylation of the C6-OH of **36**−**40** with various chain lengths of ethyl or methyl bromoalkanoate yielded ester products **41**−**51**. Conversion

Scheme 1[a]

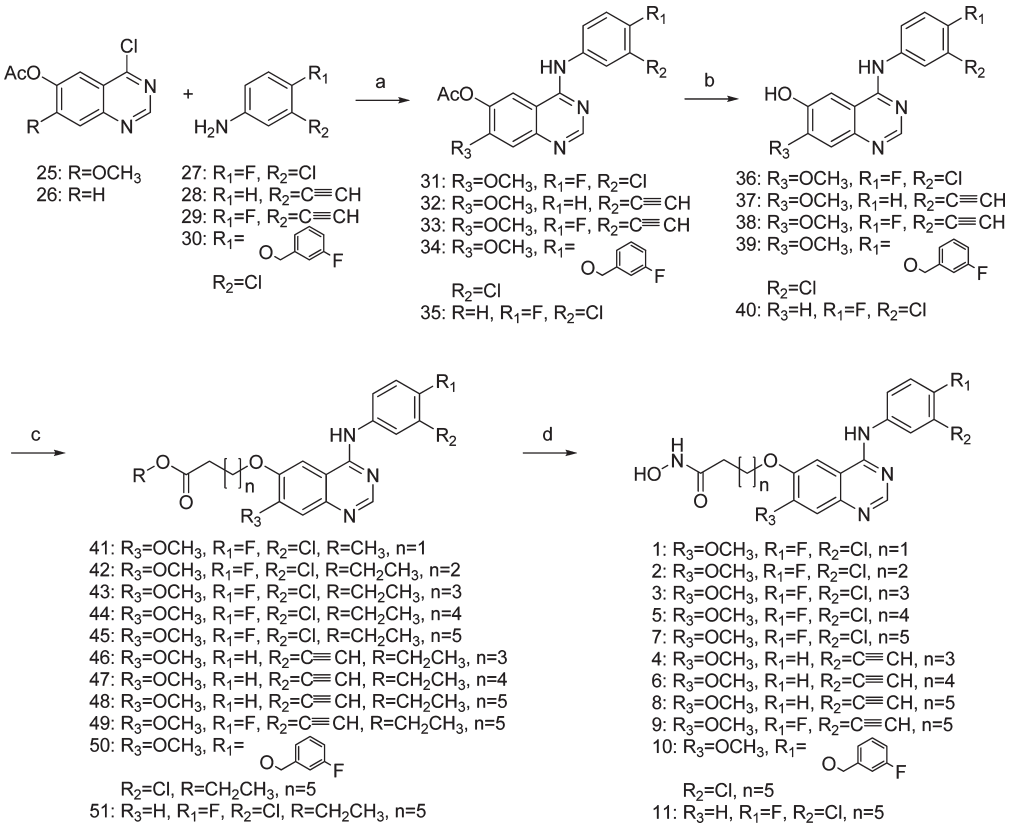

[a] (a) Isopropanol, reflux; (b) LiOH, CH_3OH, H_2O; (c) ethyl or methyl bromoalkanoate, K_2CO_3, 40 °C; (d) NH_2OH, CH_3OH, 0 °C to rt.

Scheme 2[a]

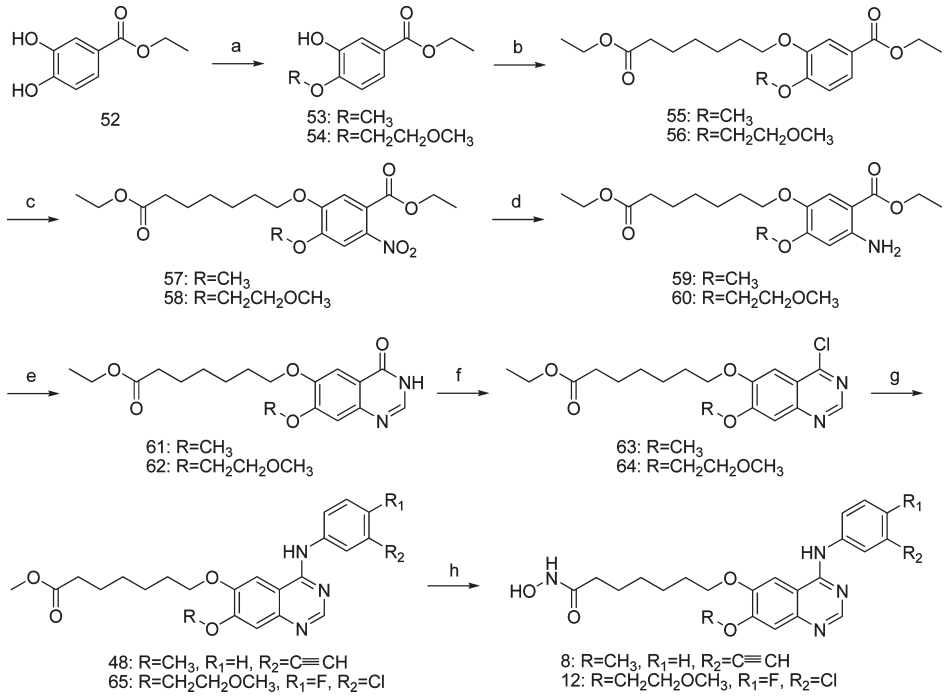

[a] (a) CH_3I or 2-methyoxyethyl-4-methylbenzenesulfonate, K_2CO_3, DMF; (b) ethyl 7-bromoheptanoate, K_2CO_3, DMF, 60 °C; (c) HNO_3, HOAc, 20 °C; (d) Fe, HCl, EtOH, H_2O, reflux; (e) $HCONH_2$, $HCOONH_4$, 180 °C; (f) PCl_3, reflux; (g) **27** or **28**, isopropanol, reflux; (h) NH_2OH, CH_3OH, 0 °C to rt.

of esters **41**−**51** to hydroxamic acids using freshly prepared hydroxylamine yielded final compounds **1**−**11**. Alternatively, these compounds may be prepared by installing the ester side chain prior to constructing the quinazoline core as shown in Scheme 2. This process is more suited to the synthesis of certain analogues and is easy to scale up. Compound **52** was treated

Scheme 3[a]

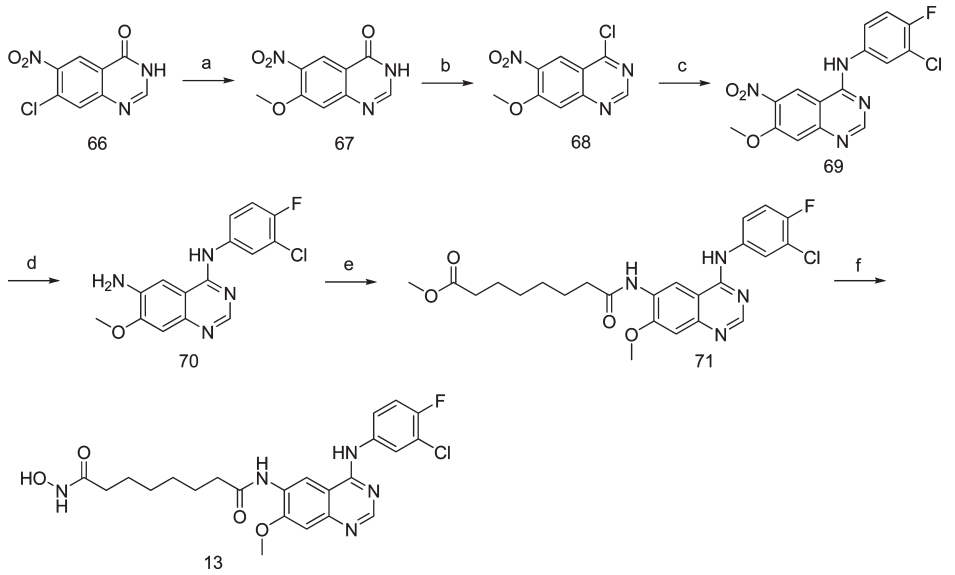

[a] (a) Na, CH_3OH, sealed tube; (b) $POCl_3$, reflux; (c) **27**, isopropanol, reflux; (d) Fe, HCl, EtOH, H_2O, reflux; (e) methyl 5-chloro-5-oxopentanoate, Et_3N, CH_2Cl_2; (f) NH_2OH, CH_3OH, 0 °C to rt.

Scheme 4[a]

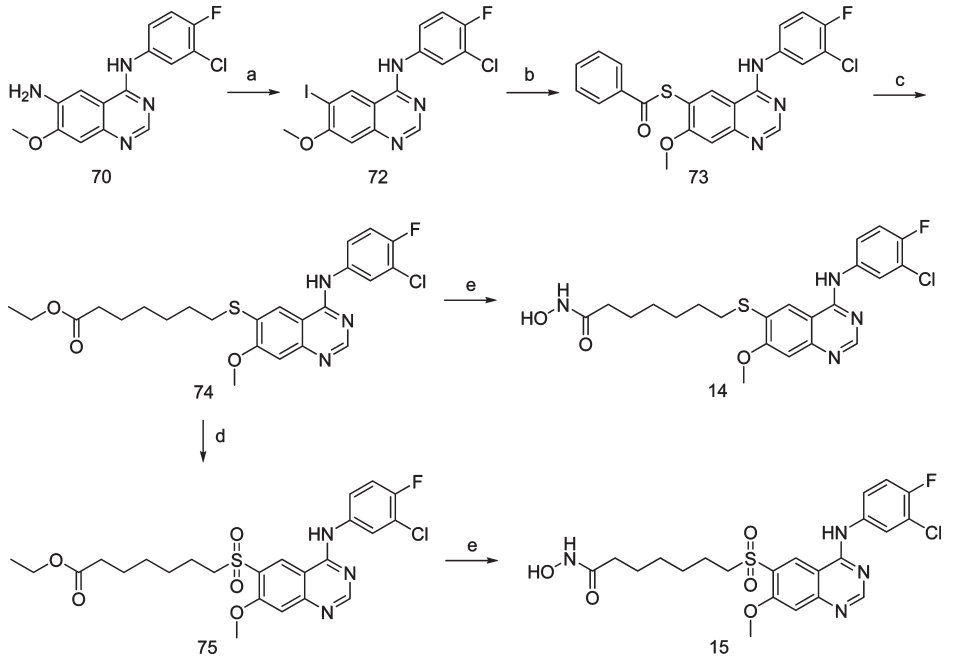

[a] (a) $NaNO_2$, H_2SO_4, AcOH, KI; (b) thiobenzoic acid, 1,10-phenathroline, CuI, DIPEA, toluene, 110 °C; (c) ethyl 7-bromoheptanoate, K_2CO_3, DMF, 50 °C; (d) $KMnO_4$, CH_3CN, H_2O, 65 °C; (e) NH_2OH, CH_3OH, 0 °C to rt.

with iodomethane or 2-methoxyethyl-4-methylbenzenesulfonate to give corresponding intermediates **53** and **54**. Alkylation of **53** and **54** with ethyl 7-bromoheptanoate gave intermediates **55** and **56**, which were then treated with fuming nitric acid to introduce a nitro group onto the phenyl ring to yield **57** and **58**. Reduction of nitro compounds **57** and **58** with iron/hydrochloric acid gave corresponding amines **59** and **60**. Cyclization of **59** and **60** using formamide and ammonium formate gave quinazoline intermediates **61** and **62**. Chlorination of **61** and **62** using phosphoryl chloride yielded the desired intermediates **63** and **64**. The coupling of **63** and **64** with **27** and **28** gave corresponding esters **48** and **65**, which were finally reacted with freshly prepared hydroxylamine to form final product **8** and **12**, respectively.

The preparation of amide linker compound **13** is shown in Scheme 3. Conversion of the chloro group of **66** to the methoxy group using in situ formed sodium methoxide gave the corresponding methoxy compound **67**. Treatment of **67** with phosphoryl chloride gave the chloride **68**. Coupling of **68** with **27** gave nitro compound **69**. Reduction of **69** with iron/hydrochloric acid gave the corresponding amine **70**. Coupling of **70** with methyl 5-chloro-5-oxopentanoate yielded amide **71**. Final compound **13** was obtained by the treatment of **71** with freshly prepared hydroxylamine.

The sulfur and sulfone-linked side chain compounds **14** and **15** were synthesized according to Scheme 4. Conversion of amino group of **70** to iodo group was achieved by first forming

Scheme 5[a]

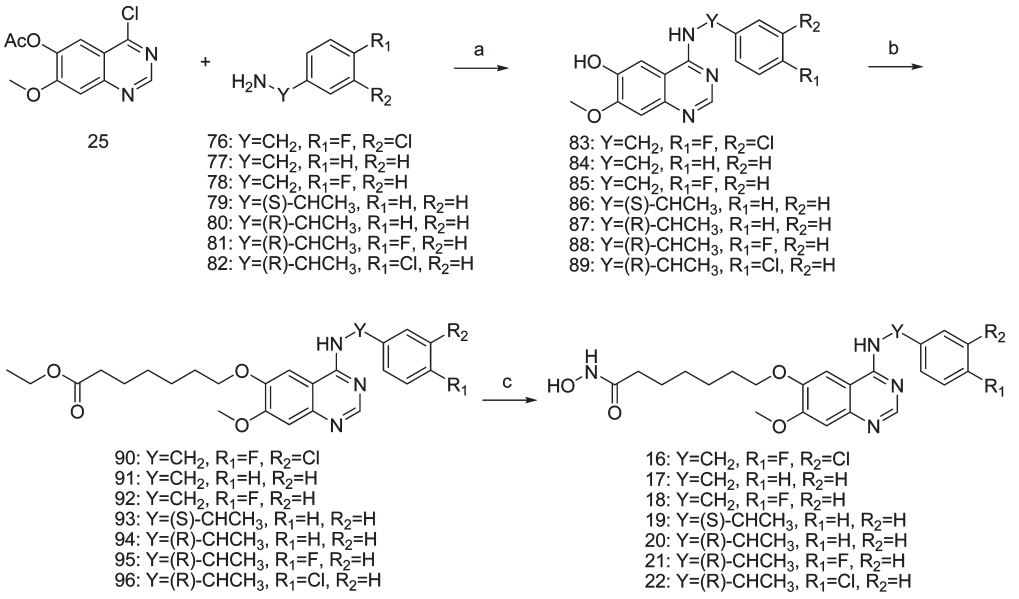

[a] (a) Isopropanol, 60 °C; (b) ethyl 7-bromoheptanoate, K_2CO_3, DMF, 60 °C; (c) NH_2OH, CH_3OH, 0 °C to rt.

a diazonium salt and subsequently reacting it with cuprous iodide to yield compound **72**. Treatment of compound **72** with thiobenzoic acid gave compound **73**. Hydrolysis of the thioester **73** using potassium carbonate generated free thio compound, which was then reacted with ethyl 7-bromoheptanoate to give compound **74**. Oxidation of **74** with $KMNO_4$ gave the sulfone intermediate **75**. Final hydroxamic acid compounds **14** and **15** were obtained by reacting esters **74** and **75** with freshly prepared hydroxylamine, respectively.

The synthesis of the benzylamine series of analogues **16**−**22** is shown in Scheme 5. Compounds **83**−**89** were synthesized by the coupling of compound **25** with commercially available amines **76**−**82.** In the reaction condition, the C-6 acetyl group was cleaved to form C-6 OH. Alkylation of the C-6 OH of **83**−**89** with ethyl 7-bromoheptanoate gave compounds **90**−**96**. Final hydroxamic acids **16**−**22** were prepared through the conversion of esters **90**−**96** using freshly prepared hydroxylamine.

The preparation of position analogues **23** and **24** is shown in Scheme 6. Alkylation of the C-4 OH of **52** with ethyl 7-bromoheptanoate gave compound **97**. Methylation of the C-3 OH of **97** using iodomethane gave compound **98**. Introduction of a nitro group onto compound **98** to form compound **99** was accomplished by treating **98** with fuming HNO_3 and AcOH. Reduction of **99** using iron/hydrochloric acid gave its corresponding amine **100**. Cyclization of **100** using formamide and ammonium formate gave the quinazoline intermediate **101**. Chlorination of **101** using phosphoryl chloride gave intermediate **102**. Coupling of **102** with anilines **27** and **28** yielded compounds **103** and **104**, respectively. Treatment of **103** and **104** with freshly prepared hydroxylamine gave the final position analogues **23** and **24**.

Results and Discussion

To study structure−activity relationships, compounds were evaluated in EGFR and HER2 kinase activity assays, as well as an HDAC enzyme assay. For the purpose of SAR analysis, all compounds were assigned to four groups including chain length and phenyl ring substitution analogues, quinazoline ring substitution analogues, benzylamine analogues, and position analogues. The in vitro enzymatic inhibition assay results of these four types of compounds are summarized in Tables 1−4.

Chain Length and Phenyl Ring Substitution Analogues (1−10, Table 1). Our data suggest that increasing the length of the hydroxamic acid side chain increases HDAC inhibitory activity. The short chain analogues (compounds **1** and **2**) have weak HDAC inhibitory activity. Appreciable HDAC inhibition was observed only when the carbon chain length between the quinazoline C-6 oxygen and the hydroxamic acid carbonyl group reached four carbons (n = 3) (compounds **3** and **4**). The HDAC inhibitory activity further increased with a carbon chain length of five carbons (n = 4) (compounds **5** and **6**). The optimal carbon chain length is six (n = 5), which gives an IC_{50} of HDAC inhibition in the single-digit nanomolar range (compounds **7**, **8**, and **9**). Small substituents on the phenyl ring do not affect the HDAC inhibitory activity, but a large group, such as 3-fluorophenylmethoxy decreases potency of HDAC inhibition (**10**, IC_{50} = 58.1 nM). These results suggest that the length of the hydroxamic acid side chain is important for HDAC inhibition. In contrast, EGFR and HER2 inhibition were largely unaffected by the change in carbon chain length and phenyl ring substitution (EGFR inhibition IC_{50}=2.4 nM − 15.1 nM; HER2 inhibition IC_{50} = 10.1 nM − 38.4 nM) with the exception of compound **9**, which had relatively low inhibitory activities against EGFR (IC_{50} = 28.8 nM) and HER2 (IC_{50} = 76.5 nM). These data suggest that the side chain on the quinazoline ring and substitution on the phenyl ring are not critical for EGFR/HER2 inhibition, and that the optimal carbon chain length to achieve maximum inhibitory activities against HDAC and EGFR/HER2 is six carbons (n = 5). Among four six-carbon chain (n = 5) compounds (**7**, **8**, **9**, **10**), **7** and **8** are more promising, with potent inhibitory activities against all three targets, HDAC, EGFR, and HER2. Compared with reference compounds, **7** and **8** inhibit HDAC and EGFR activity with higher potency than vorinostat and erlotinib (or lapatinib), respectively.

Scheme 6[a]

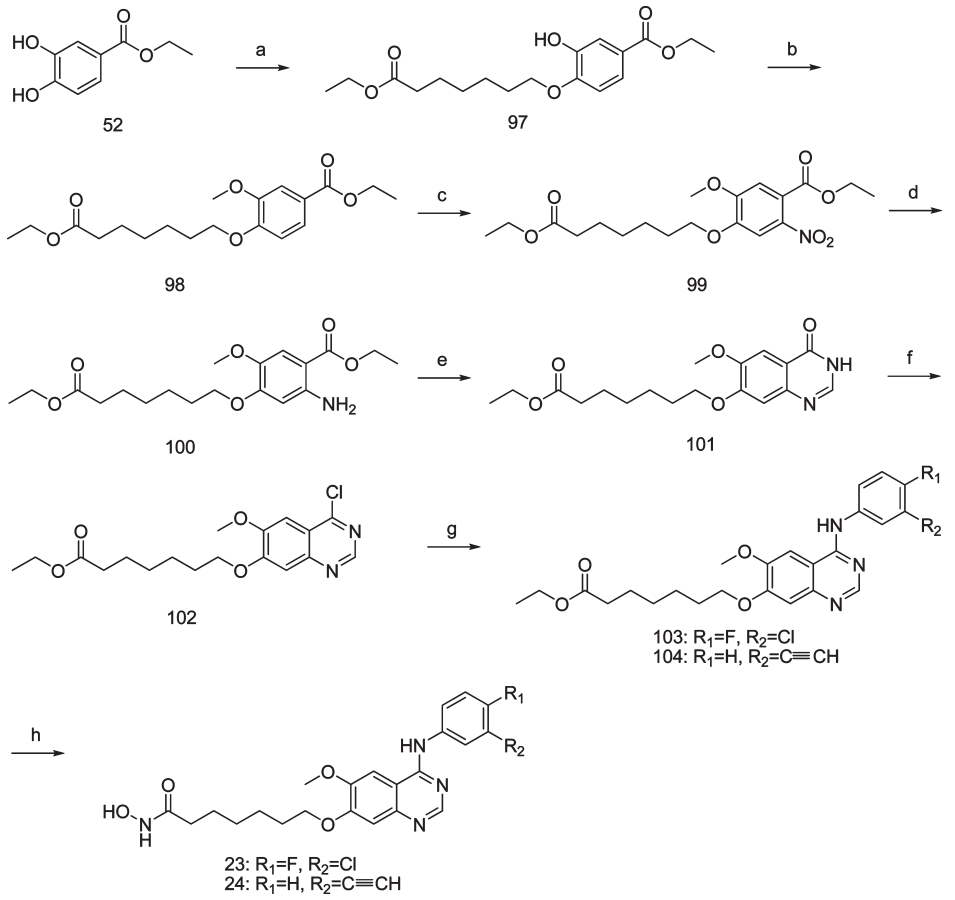

[a] (a) Ethyl 7-bromoheptanoate, K_2CO_3, DMF; (b) CH_3I, K_2CO_3, DMF, 80 °C; (c) HNO_3, AcOH, 20 °C; (d) Fe, HCl, EtOH, reflux; (e) $HCONH_2$, $HCOONH_4$, 180 °C; (f) $POCl_3$, reflux; (g) **27** or **28**, isopropanol, reflux; (h) NH_2OH, CH_3OH, 0 °C to rt.

Moreover, **7** and **8** exhibit greater or equal potency of HER2 inhibition compared to erlotinib or lapatinib, respectively.

Quinazoline Ring Substitution Analogues (7, 11−15, Table 2). Keeping the optimal carbon chain length of six (n = 5), our next step was to examine the influence of C-7 substitution (R_3) and the C-6 oxygen atom of the quinazoline ring on inhibitory activities. When X is an oxygen, varying R_3 does not affect HDAC inhibition (all such compounds displayed a single-digit nanomolar IC_{50}), while the potency of EGFR or HER2 inhibition has the following order: OCH_3 (compound **7**) > $OCH_2CH_2OCH_3$ (compound **12**) > H (compound **11**). When R_3 is fixed to be OCH_3, the linker X does affect HDAC, EGFR, and HER2 inhibitory activities. For HDAC inhibition, an oxygen linker (compound **7**) is more potent than an amide linker (compound **13**), which is more potent than a sulfur linker (compound **14**), while a sulfone linker **15** has lowest potency. For EGFR and HER2 inhibition, **7**, **13**, and **14** have similar potency, but sulfone linker **15** showed reduced potency in EGFR inhibition (IC_{50} = 15.4 nM) and greatly reduced HER2 inhibition (IC_{50} > 2000 nM).

Benzylamine Analogues (16−22, Table 3). Unlike the aniline analogues discussed earlier, the benzylamine series disrupted the conjugation of the quinazoline ring with the phenyl ring. The HDAC inhibition drops to half when changing aniline (**7**, IC_{50} = 6.5 nM) to benzylamine (**16**, IC_{50} = 11.3 nM), but is restored when R_1 and R_2 are both H (**17**, IC_{50} = 4.2 nM) or R_1 is F and R_2 is H (**18**, IC_{50} = 5.6 nM). When a methyl group is added onto the benzylamine methelene of compound **17** to create a pair of enantiomers, the S isomer shows a 6-fold drop (**19**, IC_{50} = 25.7 nM) and the R isomer shows a 23-fold drop (**20**, IC_{50} = 98.4 nM) in HDAC inhibition compared to **17**. When changing H on R_1 of compound **20** to F (**21**) or Cl (**22**), an additional 1.5- to 2-fold drop of HDAC inhibition is observed compared to compound **20**. For EGFR and HER2 inhibition, the replacement of aniline (**7**) with benzylamine (**16**) resulted in a more than 20-fold drop in EGFR and HER2 inhibition. Unlike HDAC inhibition, the R isomers (**20**, **21**, and **22**) all have much higher EGFR and HER2 inhibitory activities than the S-isomer (**19**), which shows very weak inhibitory activity against EGFR (IC_{50} = 5077 nM) and HER2 (IC_{50} > 2000 nM). Among the three R isomers, the potency of EGFR and HER2 inhibition is related to the phenyl ring substitution and has the following order: unsubstituted **20** > monofluoro-substituted 21 > monochloro-substituted **22**. Overall, the changing of an aniline to a benzylamine resulted in less potent compounds.

Position Analogues (7, 8, 23, 24, Table 4). To investigate the effect of the hydroxamic acid side chain position on inhibitory activities, we synthesized **23** (a position analogue of **7**) and **24** (a position analogue of **8**). Compound **23** showed a 10-fold drop in HDAC inhibition, a 2.2-fold drop in EGFR inhibition, and a 3.5-fold drop in HER2 inhibition compared to **7**. Similarly, compound **24** showed a 8-fold drop in HDAC inhibition, a 3.4-fold drop in EGFR inhibition, and a 3.3-fold drop in HER2 inhibition compared to compound **8**.

The SAR study led to the identification of compound **7** and **8** as the most potent compounds in inhibiting HDAC, EGFR, and HER2. In addition, these two compounds display balanced inhibitory activities against all three targets, a desirable feature

Table 1. Structure and In Vitro Activity of Chain Length and Ring Substitution Analogues

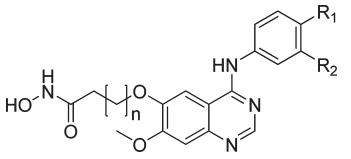

Compd	n	R1	R2	IC_{50} (nM) in Enzyme Assays HDAC[b]	EGFR[c]	HER2[c]
1	1	F	Cl	40900	7.1	10.6
2	2	F	Cl	>100000	7.8	12.4
3	3	F	Cl	551.0	9.4	15.0
4	3	H	C≡CH	421.0	15.0	38.4
5	4	F	Cl	31.0	3.4	20.0
6	4	H	C≡CH	13.2	4.6	38.2
7	5	F	Cl	6.5	3.1	19.0
8	5	H	C≡CH	4.4	2.4	15.7
9	5	F	C≡CH	3.4	28.8	76.5
10	5		Cl	58.1	9.08	10.1
vorinostat[a]				40.0	N/A	N/A
erlotinib[a]				N/A	48.0	134.5
lapatinib[a]				N/A	11.2	10.2

[a] Synthesized in-house. [b] HDAC inhibitory activity was determined using the Biomol Color de Lys system. [c] EGFR and HER2 kinase activity was measured using HTScan EGF receptor and HER2 kinase assay kits (Cell Signaling Technology).

Table 2. Structure and In Vitro Activity of Quinazoline Ring Substitution Analogues

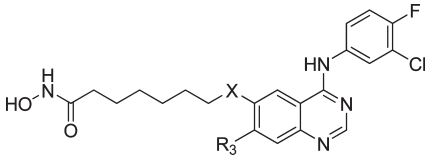

compd	X	R_3	IC_{50} (nM) in enzyme assays HDAC[a]	EGFR[b]	HER2[b]
7	O	CH_3O-	6.5	3.1	19.0
11	O	H-	4.4	84.2	43.5
12	O	$CH_3OCH_2CH_2O$-	8.4	10.4	24.0
13	CONH	CH_3O-	15.3	2.1	20.1
14	S	CH_3O-	39.6	1.99	24.2
15	SO_2	CH_3O-	121.7	15.4	> 2000

[a] HDAC inhibitory activity was determined using the Biomol Color de Lys system. [b] EGFR and HER2 kinase activity was measured using HTScan EGF receptor and HER2 kinase assay kits (Cell Signaling Technology).

Table 3. Structure and In Vitro Activity of Right-Side Phenyl Ring Analogues

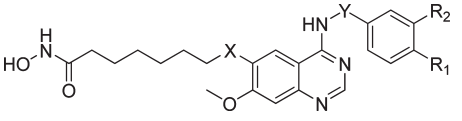

compd	Y	R_1	R_2	IC_{50} (nM) in Enzyme Assays HDAC[a]	EGFR[b]	HER2[b]
7	direct bond	F	Cl	6.5	3.1	19.0
16	CH_2	F	Cl	11.3	72.0	478.2
17	CH_2	H	H	4.2	99.4	225.2
18	CH_2	F	H	5.6	268.0	295.4
19	(S)-$CHCH_3$	H	H	25.7	5077.0	> 2000
20	(R)-$CHCH_3$	H	H	98.4	12.8	27.8
21	(R)-$CHCH_3$	F	H	165.3	125.6	175.0
22	(R)-$CHCH_3$	Cl	H	188.0	614.0	556.9

[a] HDAC inhibitory activity was determined using the Biomol Color de Lys system. [b] EGFR and HER2 kinase activity was measured using HTScan EGF receptor and HER2 kinase assay kits (Cell Signaling Technology).

for a multitargeted inhibitor. We further evaluated these two compounds, along with other selected compounds from the above SAR studies, for their antiproliferative effects on tumor cells. In NSCLC, liver, breast, and pancreatic cancer cell lines, compound **8** consistently exhibits greater potency than compound **7** (Table 5). Compound **8** was further evaluated in a series of in vitro cell-based assays, selectivity assays, in vivo efficacy models and PK/PD, metabolism, and toxicology studies.[20] Here, we describe the salient properties of this compound.

In vitro, **8** inhibits both class I and class II HDACs (Supporting Information Table S2), but not class III, Sir-type HDACs (data not shown). **8** displays broad antiproliferative

Table 4. Structure and In Vitro Activity of Side Chain Position Analogues

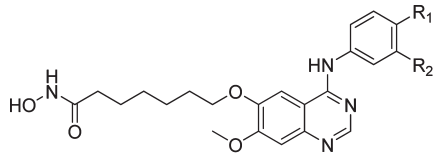

7 - 8

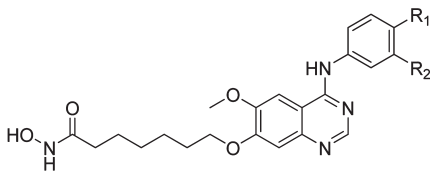

23 - 24

			IC_{50} (nM) in enzyme assays		
compd	R1	R2	HDAC[a]	EGFR[b]	HER2[b]
7	F	Cl	6.5	3.1	19.0
23	F	Cl	66.6	7.0	71.2
8	H	C≡CH	4.4	2.4	15.7
24	H	C≡CH	34.1	8.2	51.6

[a] HDAC inhibitory activity was determined using the Biomol Color de Lys system. [b] EGFR and HER2 kinase activity was measured using HTScan EGF receptor and HER2 kinase assay kits (Cell Signaling Technology).

Table 5. Inhibition of Proliferation in Selected Human Cancer Cell Lines by Compound **8**, **7**, and Reference Compounds

		IC_{50} (uM)[a]						
cancer type	cell line	**8**	**7**	vorinostat	erlotinib	vorinostat + erlotinib	lapatinib	vorinostat + lapatinib
NSCLC	HCC827	0.60	0.93	1.80	7.50	2.3		
NSCLC	H358	0.40	0.71	2.50	6.00	1.10		
NSCLC	H460	0.70	0.90	1.70	8.20	1.40		
Liver	HepG2	0.13	0.29	1.66	> 20	1.95	6.27	1.23
Liver	Hep3B2	0.23	0.60	2.44	> 20	2.64	5.49	2.36
Liver	Sk-Hep-1	0.22	0.33	3.46	10.37	3.97	5.30	1.50
Pancreatic	Capan1	0.80	1.73	7.30	> 20	4.40		
Pancreatic	BxPc3	0.27	0.38	2.70	7.60	1.00		
Breast	MCF-7	0.55	1.10	2.80	> 20	2.70	6.60	2.60
Breast	MDA-MB-231	0.10	0.37	2.11	> 20	2.00	5.40	1.80
Breast	Sk-Br-3	0.04	0.17	1.19	1.56	0.90	0.04	0.05

[a] Cancer cell lines were plated at 5000 to 10 000 cells per well in 96-well flat-bottomed plates with varying concentrations of compounds. The cells were incubated with compounds for 72 h in the presence of 0.5% of fetal bovine serum. Growth inhibition was assessed by an adenosine triphosphate (ATP) content assay using the Perkin-Elmer (Waltham, MA) ATPlite kit.

activity in many human cancer cell types and in most cases has a higher potency than erlotinib, lapatinib, and combinations of vorinostat with either erlotinib or lapatinib (Table 5).[20] **8** is a potent and selective HDAC, EGFR, and HER2 inhibitor with only weak inhibition of the following protein kinases (IC_{50}): KDR (VEGFR2) (849 nM), Src (11000 nM), Lyn (840 nM), Lck (5910 nM), Abl-1 (2890 nM), FGFR-2 (3430 nM), Flt-3 (1500 nM), and Ret (3200 nM).

In vivo, **8** induces tumor regression in the Hep-G2 liver cancer model and is more efficacious than erlotinib at its maximum tolerated dose (MTD)[20] and vorinostat at an equimolar concentration dose (Figure 2, Table 6). **8** is also highly efficacious in a number of other xenograft models (Table 6). In the erlotinib-resistant A549 NSCLC xenograft model, **8** shows potent inhibition of tumor growth. In the erlotinib-sensitive H358 NSCLC models, **8** inhibits tumor growth in a dose-dependent manner. **8** causes significant tumor regression in the lapatinib-resistant, HER2-negative, EGFR-overexpressing MDA-MB-468 breast cancer model and the EGFR-overexpressing CAL-27 head and neck squamous cell carcinoma (HNSCC) model. **8** also inhibits tumor growth in the K-ras mutant HCT116 colorectal and EGFR/HER2 (neu)-expressing HPAC pancreatic cancer models.

Our studies on the mechanism of action suggest that **8** may overcome drug resistance via the sustained blockade of survival pathways. We have demonstrated that besides EGFR and HER2 inhibition, **8** also suppresses HER3 expression, Met amplification, and AKT reactivation in tumor cells.[20]

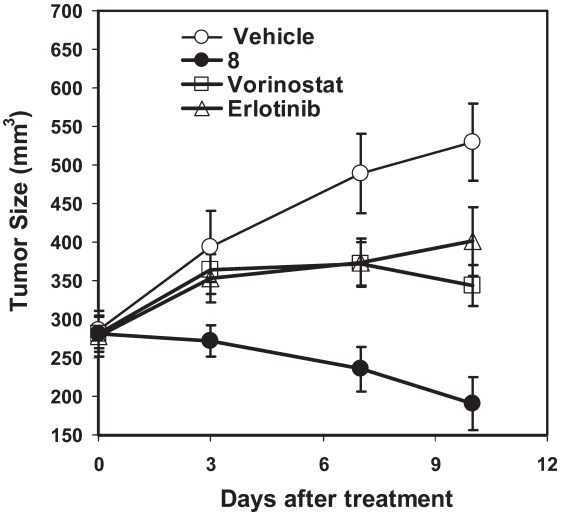

Figure 2. **8**, dosed at 120 mg/kg, iv, daily, induced tumor regression in the Hep-G2 liver cancer model and was more efficacious than erlotinib at its maximum tolerated dose (MTD, 25 mg/kg, po, daily) and vorinostat at an equimolar concentration (72 mg/kg, iv, daily).

In conclusion, compound **8** is a potent HDAC, EGFR, and HER2 inhibitor with favorable drug-like properties. It

Table 6. In Vivo Efficacy of Compound **8** in Mice Human Tumor Xenograft Models

cancer type	cell line	dosing schedule[a]	T/C % or regression (−)[b]
NSCLC	H358	**8**, 15 mg/kg	41.9
		8, 30 mg/kg	10.3
		8, 60 mg/kg	6.5
	A549	**8**, 120 mg/kg	35.9
breast	MDA-MB468	**8**, 120 mg/kg	−13.7
		Lapatinib,75 mg/kg	51.0
colon	HCT116	**8**, 60 mg/kg	35.3
HNSCC	CAL-27	**8**, 120 mg/kg	−36.5
liver	HepG2	**8**, 120 mg/kg	−21.3
		Erlotinib, 25 mg/kg	50.8
		Vorinostat, 72 mg/kg	26.0
pancreatic	HPAC	**8**, 120 mg/kg	35.1

[a] Compound **8** was dosed iv, daily, except in the H358 NSCLC model, where **8** was dosed iv on 7−6−5 (on−off−on) schedule, and in HCT116 colorectal cancer model, **8** was dosed iv on 5−2−5 (on−off−on) schedule. Lapatinib was dosed po, bid. Erlotinib was dosed po, daily, and vorinostat was dosed iv, daily. [b] During each animal study, tumors were measured with calipers, tumor size determined using the formula: tumor volume = (length × width^2)/2, and tumor size changes in percent calculated. In most cases, % T/C values were calculated using the following formula: % $T/C = 100 \times \Delta T/\Delta C$ if $\Delta T > 0$, where T/C is the tumor size change ratio in treated animals (T) and control animals (C), ΔT is the tumor size change in treated animal between last tumor size measurement and predosing (T_0) tumor size measurement, ΔC is the tumor size change in control animal between last tumor size measurement and predosing tumor size measurement. In cases where tumor regression occurred ($\Delta T < 0$), however, the following formula was used: % $T/T_0 = 100 \times \Delta T/T_0$, where T/T_0 is the tumor size change ratio in treated animal. Values of $< 42\%$ are considered significant.[32]

also displays a favorable preclinical safety profile (data not shown). Its simultaneous blockade of HDAC and RTK pathways represents a novel approach to cancer therapy and may provide high efficacy and overcome limitations in the treatment of certain cancers with RTK inhibitors. Therefore, compound **8** has advanced to clinical development as a novel anticancer agent.

Experimental Section

Chemistry. Anhydrous solvents and other solvents were purchased from commercial suppliers. All other chemicals were from commercial suppliers and used without further purification. ^{1}H NMR spectra were recorded on a Bruker AVANCE III 400 MHz or Varian Mercury-VX-300 300 MHz NMR spectrometer at ambient temperature and proton chemical shifts are relative to TMS as an internal standard. Melting points were determined on a X-4 micromelting point apparatus in microscope slides and cover glass, or a WRS-1B digital melting point apparatus in an open capillary tube and are uncorrected (both melting point apparatuses were manufactured by Shanghai Precision & Scientific Instrument Co., Ltd.).

LCMS. The purity of the compounds was analyzed by reversed-phase liquid chromatography and mass spectrometry (Agilent 6110 quadruple ion trap mass spectrometer or Shimadzu LCMS-2010EV chromatograph mass spectrometer) with a UV detector at 214 and 254 nm and electrospray ionization source (ESI) as described in further detail in the Supporting Information. All final compounds (**1**−**24**) were assayed by LCMS methods and showed purity of at least 95%.

Preparative HPLC. The separation of certain compounds was accomplished by using reverse-phase preparative HPLC (Gilson GX-281) with a UV detector at 214 nm as described in further detail in the Supporting Information.

General Procedure for the Synthesis of 31−**35.** A mixture of 4-chloroquinazolines derivatives (**25**−**26**, 5 mmol) and appropriate substituted anilines (**27**−**30**, 10 mmol) in isopropanol (45 mL) was stirred at reflux for 3 h. The reaction mixture was cooled to room temperature and the resultant precipitate was collected by filtration. The solid was further dried in vacuo to give the compounds **31**−**35**.

General Procedure for the Synthesis of 36−**40.** A mixture of 4-phenylamino-quinazoline derivatives (**31**−**35**, 3.5 mmol) and $LiOH \cdot H_2O$ (0.5 g, 11.7 mmol) in methanol (100 mL) and H_2O (100 mL) was stirred at room temperature for 0.5 h. The mixture was neutralized by the addition of diluted acetic acid. The resultant precipitate was collected by filtration, washed, and dried to give compounds **36**−**40**.

General Procedure for the Synthesis of 41−**51.** A mixture of 4-phenylaminoquinazolin-6-ol derivatives (**36**−**40**, 1.0 mmol), appropriate ethyl or methyl bromoalkanoate (1.1 mmol), and potassium carbonate (323 mg, 2.4 mmol) in DMF (6 mL) was stirred at 40 °C for 30 min. The reaction mixture was filtered and the filtrate was concentrated in vacuo. The residue was washed with diethyl ether and dried to give compounds **41**−**51**.

General Procedure for the Synthesis of 1−**24 from Their Corresponding Esters. Preparation of Fresh Hydroxylamine solution.** A solution of potassium hydroxide (11.2 g, 199.6 mmol) in methanol (28 mL) was added to a stirred solution of hydroxylamine hydrochloride (9.34 g, 134.4 mmol) in methanol (48 mL) at 0 °C. The reaction mixture was stirred at 0 °C for 30 min. The resultant precipitate was removed by filtration. The filtrate was collected to provide free hydroxylamine solution which was stored in a refrigerator before use.

Preparation of Compounds 1−**24.** The appropriate esters (11.0 mmol) were added to the above freshly prepared hydroxylamine solution (30 mL) at 0 °C. The reaction mixture was warmed to room temperature and stirred at 25 °C for 1 to 24 h until the reaction was complete (reaction progess was monitored by TLC or LCMS). The reaction mixture was neutralized with acetic acid. The formed precipitate was collected by filtration, washed with water, and dried to give the title compounds. If a precipitate did not form after neutralization, the solvent was removed to yield a crude mixture, which was purified by reverse-phase preparative HPLC to give the title compounds.

EGFR and HER2 Inhibition Assay. EGFR and HER2 kinase activity were measured using HTScan EGF receptor and HER2 kinase assay kits (Cell Signaling Technology). Briefly, the GST-EGFR fusion protein was incubated with synthetic biotinylated peptide substrate and varying concentrations of drugs in the presence of 400 mM ATP. Phosphorylated substrate was captured with strapavidin-coated 96-well plates. The level of phosphorylation was monitored by antiphospho-tyrosine- and europium-labeled secondary antibodies (DELFIA, Perkin-Elmer). The enhancement solution was added at the end of the assay and enzyme activity was measured in the Wallac Victor II 1420 microplate reader at 615 nM.

HDAC Inhibition Assay. The activities of Class I and II HDACs were assessed using the Biomol Color de Lys system. Briefly, HeLa cell nuclear extracts were used as a source of HDACs. Different concentrations of drugs were added to HeLa cell nuclear extracts in the presence of a colorimetric artificial substrate. Developer was added at the end of the assay and enzyme activity was measured in the Wallac Victor II 1420 microplate reader at 405 nM.

Cell Growth, Viability, and Apoptosis Assay. Cancer cell lines were plated at 5000 to 10 000 cells per well in 96-well flat-bottomed plates with varying concentrations of compounds. The cells were incubated with compounds for 72 h in the presence of 0.5% of fetal bovine serum. Growth inhibition was assessed by an adenosine triphosphate (ATP) content assay using the Perkin-Elmer (Waltham, MA) ATPlite kit. Apoptosis was routinely assessed by measuring the activities of Caspase-3 and -7 using Promega (Madison, WI) Apo-ONE Homogeneous Assay Kit.

Efficacy Studies in Human Cancer Xenograft Model. Four- to six-week-old female athymic mice (nude nu/nu CD-1, Charles

River, Wilmington, MA) were inoculated subcutaneously into the right hind flank region with 1 to 5×10^6 cells in a medium suspension of 100−200 μL. For orthotopic implantation of breast cancer cells, a cell suspension in 100 μL of medium was injected directly into the mammary fat pads through a 27G needle. Different doses of **8**, standard anticancer agents and vehicle were administered orally, intraperitoneally, or via tail vein injection as indicated.

Acknowledgment. The authors thank Zihong Guo, Tianhao Wang, Keyou Xue, Hui Liu, Xiaoyue Su, Xiongwen Yang and Liangbin Jia of Curis chemistry FTE team at Shanghai ChemPartner Co., Ltd. for conducting chemical synthesis of compounds, Carmen Pepicelli and Mark Noel of Curis for helpful discussions and their review of this manuscript, and Nicole Davis for her assistance in the preparation of this manuscript.

Supporting Information Available: Details of synthesis and analytical data, the LCMS method used for the determination of purity and the HPLC method used for compound separation, HDAC and RTK inhibition synergy data, HDAC class I and class II inhibitory activity of **8**. This material is available free of charge via the Internet at http://pubs.acs.org.

References

(1) Sergina, N. V.; Moasser, M. M. The HER Family and Cancer: Emerging Molecular Mechanisms and Therapeutic Targets. *Trends Mol. Med.* **2007**, *13*, 527–534.
(2) Hynes, N. E; Lane, H. A. ERBB Receptors and Cancer: the Complexity of Targeted Inhibitors. *Nat. Rev. Cancer* **2005**, *5*, 341–354.
(3) Moasser, M. M. Targeting the Function of the HER2 Oncogene in Human Cancer Therapeutics. *Oncogene* **2007**, *26*, 6577–6592.
(4) Moasser, M. M. The Oncogene HER2: Its Signaling and Transforming Functions and Its Role in Human Cancer Pathogenesis. *Oncogene* **2007**, *26*, 6469–6487.
(5) Burgess, A. W.; Cho, H.-S.; Eigenbrot, C.; Ferguson, K. M.; Garrett, T. P. J.; Leahy, D. J.; Lemmon, M. A.; Sliwkowski, M. X.; Ward, C. W.; Yokoyama, S. An Open-and-shut Case? Recent Insights Into the Activation of EGF/ErbB Receptors. *Mol. Cell* **2003**, *12*, 541–552.
(6) Press, M. F.; Lenz, H.-J. EGFR, HER2 and VEGF Pathways: Validated Targets for Cancer Treatment. *Drugs* **2007**, *67*, 2045–2075.
(7) Sharma, S. V.; Bell, D. W.; Settleman, J.; Haber, D. A. Epidermal Growth Factor Receptor Mutations in Lung Cancer. *Nat. Rev. Cancer* **2007**, *7*, 169–181.
(8) Zhang, H.; Berezov, A.; Wang, Q.; Zhang, G.; Drebin, J.; Murali, R.; Greene, M. I. ErbB Receptors: from Oncogenes to Targeted Cancer Therapies. *J. Clin. Invest.* **2007**, *117*, 2051–2058.
(9) Pao, W.; Miller, V. A.; Politi, K. A.; Riely, G. J.; Somwar, R.; Zakowski, M. F.; Kris, M. G.; Varmus, H. Acquired Resistance of Lung Adenocarcinomas to Gefitinib or Erlotinib is Associated with a Second Mutation in the EGFR Kinase Domain. *PLoS Med.* **2005**, *2*, e73.
(10) Avizienyte, E.; Ward, R. A.; Garner, A. P. Comparison of the EGFR Resistance Mutation Profiles Generated by EGFR-targeted Tyrosine Kinase Inhibitors and the Impact of Drug Combinations. *Biochem. J.* **2008**, *415*, 197–206.
(11) Rubin, B. P.; Duensing, A. Mechanisms of Resistance to Small Molecule Kinase Inhibition in the Treatment of Solid Tumors. *Lab. Invest.* **2006**, *86*, 981–986.
(12) Marks, P. A.; Xu, W.-S. Histone Deacetylase Inhibitors: Potential in Cancer Therapy. *J. Cell. Biochem.* **2009**, *107*, 600–608.
(13) Pandolfi, P. P. Histone Deacetylases and Transcriptional Therapy with Their Inhibitors. *Cancer Chemother. Pharmacol.* **2001**, *48* (Suppl 1), S17–19.
(14) Mann, B. S.; Johnson, J. R.; Cohen, M. H.; Justice, R.; Pazdur, R. FDA Approval Summary: Vorinostat for Treatment of Advanced Primary Cutaneous T-cell Lymphoma. *Oncologist* **2007**, *12*, 1247–1252.
(15) Qian, D. Z.; Wang, X.; Kachhap, S. K.; Kato, Y.; Wei, Y.; Zhang, L.; Atadja, P.; Pili, R. The Histone Deacetylase Inhibitor NVP-LAQ824 Inhibits Angiogenesis and Has a Greater Antitumor Effect in Combination with the Vascular Endothelial Growth Factor Receptor Tyrosine Kinase Inhibitor PTK787/ZK222584. *Cancer Res.* **2004**, *64*, 6626–6634.
(16) Bali, P.; Pranpat, M.; Swaby, R.; Fiskus, W.; Yamaguchi, H.; Balasis, M.; Rocha, K.; Wang, H.-G.; Victoria, Richon; Kapil, Bhalla . Activity of Suberoylanilide Hydroxamic Acid Against Human Breast Cancer Cells with Amplification of Her-2. *Clin. Cancer Res.* **2005**, *11*, 6382–6389.
(17) Bali, P.; George, P.; Cohen, P.; Tao, J.; Guo, F.; Sigua, C.; Vishvanath, A.; Scuto, A.; Annavarapu, S.; Fiskus, W.; Moscinski, L.; Atadja, P.; Bhalla, K. Superior Activity of the Combination of Histone Deacetylase Inhibitor LAQ824 and the FLT-3 Kinase Inhibitor PKC412 Against Human Acute Myelogenous Leukemia Cells with Mutant FLT-3. *Clin. Cancer Res.* **2004**, *10*, 4991–4997.
(18) Edwards, A.; Li, J.; Atadja, P.; Bhalla, K.; Haura, E. B. Effect of the Histone Deacetylase Inhibitor LBH589 Against Epidermal Growth Factor Receptor-dependent Human Lung Cancer Cells. *Mol. Cancer Ther.* **2007**, *6*, 2515–2524.
(19) Fuino, L.; Bali, P.; Wittmann, S.; Donapaty, S.; Guo, F.; Yamaguchi, H.; Wang, H.-G.; Atadja, P.; Bhalla, K. Histone Deacetylase Inhibitor LAQ824 Down-regulates Her-2 and Sensitizes Human Breast Cancer Cells to Trastuzumab, Taxotere, Gemcitabine, and Epothilone B. *Mol. Cancer Ther.* **2003**, *2*, 971–984.
(20) Lai, C.-J.; Bao, R.; Tao, X; Wang, J.; Atoyan, R.; Qu, H; Wang, D.-G.; Yin, L; Samson, M; Forrester, J; Zifcak, B.; Xu, G.-X.; DellaRocca, S.; Zhai, H.-X.; Cai, X; Qian, C. CUDC-101, a Multitargeted Inhibitor of HDAC, EGFR and HER2, with Potent in vitro and in vivo Anti-cancer Activity. Unpublished results.
(21) Yu, C.; Friday, B. B.; Lai, J.-P.; McCollum, A.; Atadja, P.; Roberts, L. R.; Adjei, A. A. Abrogation of MAPK and Akt Signaling by AEE788 Synergistically Potentiates Histone Deacetylase Inhibitor-Induced Apoptosis through Reactive Oxygen Species Generation. *Clin. Cancer Res.* **2007**, *13*, 1140–1148.
(22) Chou, T. C; Talalay, P. Quantitative Analysis of Dose-effect Relationships: the Combined Effects of Multiple Drugs or Enzyme Inhibitors. *Adv. Enzyme Regul.* **1984**, *22*, 27–55.
(23) Bolden, J. E.; Peart, M. J.; Johnstone, R. E. Anticancer Activities of Histone Deacetylase Inhibitors. *Nat. Rev. Drug Discovery* **2006**, *5*, 769–784.
(24) Keri, G.; Orfi, L.; Eros, D.; Hegymegi-Barakonyi, B.; Szantai-Kis, C.; Horvath, Z.; Waczek, F.; Marosfalvi, J.; Szabadkai, I.; Pato, J.; Greff, Z.; Hafenbradl, D.; Daub, H.; Muller, G.; Klebl, B.; Ullrich, A. Signal Transduction Therapy with Rationally Designed Kinase Inhibitors. *Curr. Signal Transduction Ther.* **2006**, *1*, 67–95.
(25) Acharya, M. R.; Sparreboom, A.; Venitz, J.; Figg, W. D. Rational Development of Histone Deacetylase Inhibitors as Anticancer Agents: A Review. *Mol. Pharmacol.* **2005**, *68*, 917–932.
(26) Collins, I.; Workman, P. Design and Development of Signal Transduction Inhibitors for Cancer Treatment: Experience and Challenges with Kinase Targets. *Curr. Signal Transduction Ther.* **2006**, *1*, 13–23.
(27) Stamos, J.; Sliwkowski, M. X.; Eigenbrot, C. Structure of the Epidermal Growth Factor Receptor Kinase Domain Alone and in Complex with a 4-Anilinoquinazoline Inhibitor. *J. Biol. Chem.* **2002**, *48*, 46265–46272.
(28) Wang, D.-F.; Helquist, P.; Wiech, N. L.; Wiest†, O. Toward Selective Histone Deacetylase Inhibitor Design: Homology Modeling, Docking Studies, and Molecular Dynamics Simulations of Human Class I Histone Deacetylases. *J. Med. Chem.* **2005**, *48*, 6936–6947.
(29) Finnin, M. S.; Donigian, J. R.; Cohen, A.; Richon, V. M.; Rifkind, R. A.; Marks, P. A.; Breslow, R.; Pavletich, N. P. Structures of a Histone Deacetylase Homologue Bound to the TSA and SAHA Inhibitors. *Nature* **1999**, *401*, 188–193.
(30) Gibson, K. H. Quinazoline Derivatives. U.S. Patent 5,770,599, **1998**.
(31) Barker, A. J. Quinazoline Derivatives Useful for Treatment of Neoplastic Disease. U.S. Patent5,457,105, **1995**.
(32) Alley, M. C.; Hollingshead M. D.; Dykes D. Human Tumor Xenograft Models in NCI Drug Development. In *Anticancer drug development guide*; Teicher B. A., Andrews P. A., Eds.; Humana Press Inc.: Totowa, NJ, 2004; pp 125−152.